Intercomparison of Meteorological Forcing Data from Empirical and Mesoscale Model Sources in the N.F. American River Basin in northern California

Nicholas E. Wayand

A thesis
submitted in partial fulfillment of the
requirements for the degree of

Master of Science

University of Washington
2012

Committee:
Jessica Lundquist
Alan Hamlet

Program Authorized to Offer Degree:

Civil and Environmental Engineering

University of Washington

Abstract

Intercomparison of Meteorological Forcing Data from Empirical and Mesoscale Model Sources in the N.F. American River Basin in northern California

Nicholas Earl Wayand

Chair of the Supervisory Committee:
Professor Jessica Lundquist
Civil and Environmental Engineering

The availability of forcing data required to drive distributed hydrological models is significantly limited within mountainous terrain and at higher elevations due to the spatial scarcity of observations. Previous studies have commonly used three methods of estimating and distributing forcing data within basins that have sparse in-situ observations: a) one or two low-elevation stations in combination with empirical models, b) gridded output from a mesoscale model, or c) a combination of the two. In this study, we evaluated each source of forcing data within the heavily instrumented North Fork American River Basin in California. For the mesoscale model source, we selected the Weather Research and Forecasting (WRF) model, which used lateral boundary conditions from the North American Regional Reanalysis. Finally, each case of forcing data was used to drive the Distributed Hydrology Soil and Vegetation Model (DHSVM), and we examined those variables whose sources resulted in significant differences in simulated snowpack and streamflow.

Results indicated that the choice of the least biased forcing source was not uniform for every variable. Accumulated precipitation was dependent on the year examined, however, it is important that the WRF model performed as well as the single station combined with the climatological weighting from the Parameter Regression on Independent Slopes Model (PRISM). Simulated streamflow from DHSVM was more sensitive to the source of precipitation forcing than other variables, resulting in biased high/low flow during years when the precipitation biased was high/low.

Simulations of snowpack melt rates were most sensitive to the source of radiation data used and the elevational range considered. While the empirical estimated long-wave irradiance at high-elevation sites resulted in melt rates lower than observations, at lower-elevations the same forcing caused mid-winter melt that was not observed. However, the sensitivity of simulated snowpacks at lower-elevations was significantly reduced under a forest canopy. Short-wave irradiance from the WRF model was consistently less biased than empirical estimates, especially during cloudy days. In general, these results support the use of output from the WRF model over empirical estimates, but stress the need for additional observations to allow a complete evaluation of the energy balance.

TABLE OF CONTENTS

LIST OF FIGURES

Figure Number Page

LIST OF TABLES

Table Number Page

ACKNOWLEDGEMENTS

Funding was provided by the National Science Foundation (grant EAR-0838166), by a University of Washington Program on Climate Change Graduate Fellowship, and a University of Washington Valle Fellowship. Support for in situ instrumentation and fieldwork was provided by NOAA through their Hydrometeorological Testbed (HMT) and through a Joint Institute for the study of the Atmosphere and Ocean (JISAO) grant. The author wishes to express sincere appreciation to Jessica Lundquist and Alan Hamlet for their continued advisement, Mimi Hughes for mesoscale model support, Pablo Carrasco for help during the set-up and troubleshooting of DHSVM and the many past and present members of the UW mountain hydrology research group for aid during field work and feedback on this thesis.

DEDICATION

To my parents.

INTRODUCTION

Snowpack provides drinking water to over 40% of the world's population (Meehl et al. 2007) and generates between 50-80% of total runoff within the western U.S (Dettinger 2005), making it an important resource. Simulations of snow and hydrological processes have been found to be critically dependent on the meteorological forcing data (Reed et al. 2004; Mote et al. 2005; Tobin et al. 2011). The accuracy of precipitation and air temperature data, which ultimately determine the quantity and phase (rain or snow) of modeled precipitation, directly affects the accuracy of simulated of runoff and snow accumulation, particularly at relatively small spatial scales and shorter time scales. Other meteorological forcing variables are also important. For the western slopes of the Sierra Nevada, for example, over 80% of the snow surface energy balance is controlled by net-irradiance (Marks and Dozier 1992); thus errors in downward short- and long-wave irradiance data strongly influence simulated snowpack melt rates. Although not exhaustive, Table 1 represents some common sources of forcing data used for hydrological studies within mountainous terrain. Evaluating these different sources of forcing data, however, is not a trivial task, especially in high elevation mountain basins where very limited observations of these forcing variables are typically available (Weingartner and Pearson 2001; Lundquist et al. 2003)

In this paper we examine three sources of forcing data: a) in situ observations, b) empirical models (see Section 3) and c) physically based simulations from the Weather and Research Forecasting Model (WRF, Skamarock and Klemp 2008, described in Section 3) in a well-instrumented maritime mountain basin, the North Fork of the American River Basin (NF American Basin, Figure 1) in the northern Sierra. Due to the previously-referenced dominance of the irradiance terms in the surface energy balance in this river basin (Marks and Dozier 1992),

we do not examine turbulent fluxes and wind speed sources, but focus on the sources of precipitation, temperature, relative humidity and downward short- and long-wave irradiance data. Common empirical methods for estimating the downward irradiance variables are critically dependent on the diurnal temperature range and the relative humidity used. Therefore, we also investigate these effects. Below we describe specific experiments based on the three cases from Table 1, for which specific forcing sets over the NF American Basin will be created and evaluated.

Table 1 Common Cases of meteorological forcing data sources, which are more fully described in section 3.

	T	P	RH	W	SW	LW	Examples of Prior Studies using this approach
Case 1	Limited Obs.	Limited Obs	Limited Obs	Limited Obs	Empirical, (DTR, RH)	Empirical (DTR, RH)	(Whitaker et al. 2003; Waichler and Wigmosta 2003; Surfleet et al. 2011; Kuraś et al. 2011)
Case 2	WRF	WRF	WRF	WRF	WRF	WRF	(Zhao 2009; Westrick and Storck 2002; Westrick 2001; Leung et al. 1996)
Case 3	WRF	WRF	WRF	WRF	Empirical (DTR, RH)	Empirical (DTR, RH)	(Dettinger et al. 2011; Tapash et al. 2011)

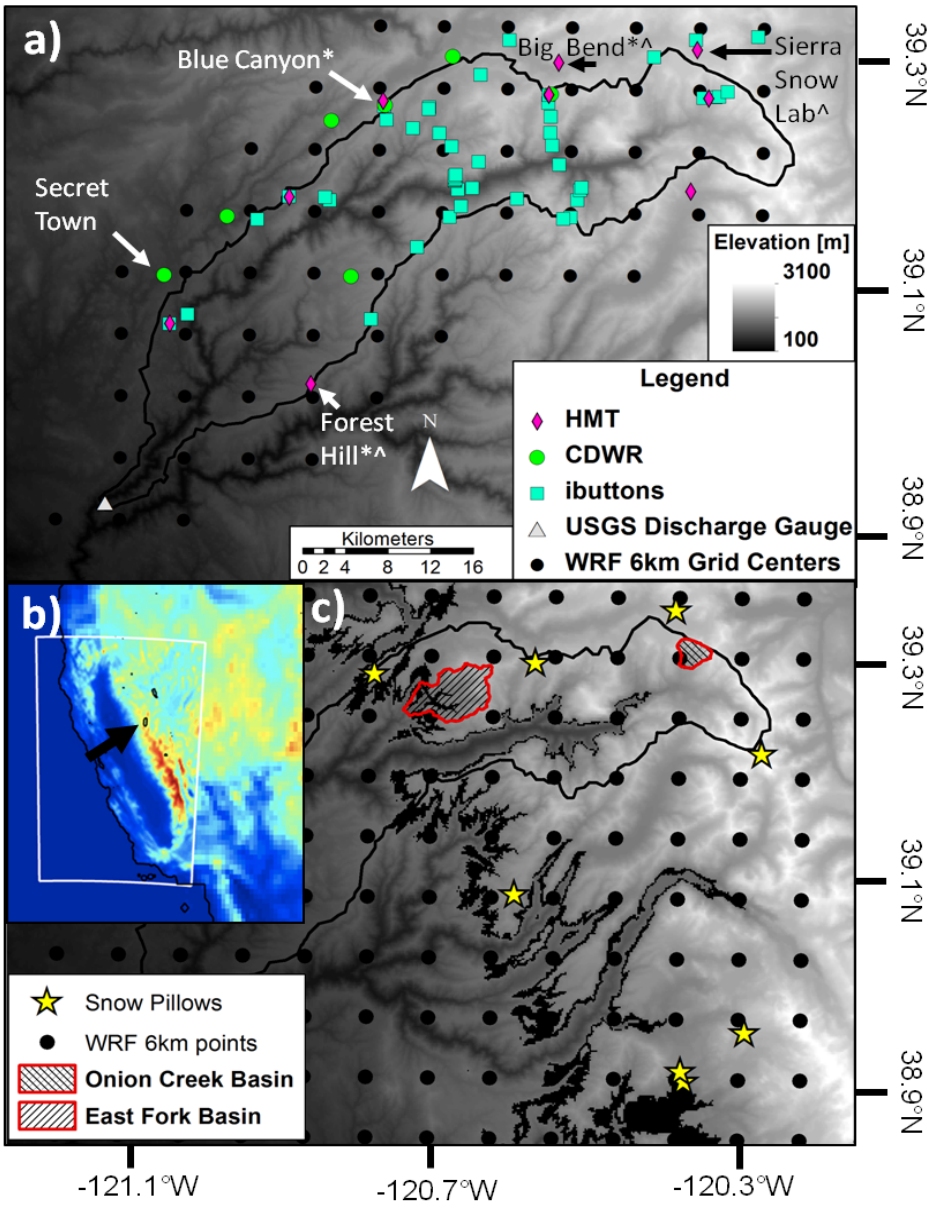

Figure 1 a) Map of the North Fork American River Basin located on the western slope of the Sierra Nevada. Shown are the meteorological stations (HMT, CDWR, and iButtons) and WRF grid cell centers used in this study. Labeled stations show stations measuring net-irradiance (*) and downward solar-irradiance (^). Center insert b) shows location of basin (*arrow*) and extent of the WRF 6km domain (*white outline*). Stars in c) show the locations of the 8 snowpillows used for model analysis. Red outlines show the boundaries of the Onion Creek and East Fork sub-basins in which stream stage was recorded. The black contour running north to south shows the climatological average snow line at 1500 meters.

Case 1 represents a study basin in which there are only one or two stations that measure precipitation, temperature and relative humidity. These point observations are then extrapolated to the entire basin using spatiotemporal weights based on historical observations from regional

studies. This methodology has been employed in studies including Waichler and Wigmosta (2003), Surfleet et al. (2011), Kuraś et al. (2011), and Whitaker et al. (2003). Table 2 highlights the typical availability of meteorological observations and common methods of estimating and distributing the unmeasured variables required for hydrological modeling. In comparison with temperature and precipitation, dew point temperature, and short- and long-wave irradiance are sparsely measured variables, which has led previous studies to estimate dew point temperature and irradiance using empirical models based on measured predictors such as the daily minimum temperature (dew point) and diurnal temperature range (short wave irradiance) (Thornton and Running 1999). Such empirical models are often fit to observed data from a particular region or climate, and their transferability to other regions has been noted as a significant limitation (Flerchinger et al. 2009).

Case 2 represents a study where only atmospheric model output is used to generate surface forcing data (e.g., Zhao 2009; Westrick 2001; Westrick and Storck 2002; Leung et al. 1996). An important advantage in using an atmospheric model is that the model can provide all meteorological variables at grid points with a greater spatial density than most observational networks. Increased spatial resolution of each grid cell has allowed numerical weather prediction models to resolve the topography that drives orographic precipitation gradients (Barros and Lettenmaier 1994; Anders et al. 2007), giving greater confidence in the underlying physical basis of the models. However, the accuracy of modeled precipitation has been shown to be sensitive to the microphysics scheme chosen (Chin et al. 2010; Dettinger et al. 2011; Minder et al. 2011). . More importantly, a more physically based estimation of downward short- and long-wave irradiance is achieved through the model's vertical representation of atmospheric moisture content, vertical temperature profile, cloud cover, etc.

Table 2 Typical variables for hydrological modeling.

	Measurement notes	Method of estimation at a point with only T and P measured	Spatially distributed	Mesoscale Model Input
Precipitation	Severe undercatch in most gages due to wind and phase of precipitation (Sevruk 1983)	Temperature used to determine fraction of solid or liquid precipitation (USACE 1956)	Often linear lapse rate (Wigmosta et al. 1994), or PRISM maps used for spatial scaling (Daly et al. 1994),	Captures large scale precipitation, atmospheric river events (Dettinger et al. 2011), and orographic effects (Barros and Lettenmaier 1994). Cannot resolve basin valley features.
Air temperature	Can be biased from location of sensor or from inadequate radiation shielding (Huwald et al. 2009).	Often hourly measurements estimated from T_{max} and T_{min} (Susong et al. 1999).	Assumed lapse rate from global average -6.5 C km^{-1} (Hamlet and Lettenmaier 1999) or from nearby stations (Susong et al. 1999) or PRISM (Daly et al. 1994).	More physically based description of mean lapse rates and how lapse rate changes with geographic location or time (Minder et al. 2010).
Vapor pressure	Few measurements; sensors prone to error and hysteresis without frequent calibration (Marks and Dozier 1992).	Assume T_{min} represents dewpoint (Running et al. 1987); large errors in arid environments (Kimball et al. 1997).	Assumed linear lapse rate from nearby stations (Susong et al. 1999) or fixed dewpoint lapse rate [-1.25 °C km^{-1}, (Running et al. 1987).	More physically based description of water vapor and how it changes with elevation and through time.
Downward short-wave (SW) irradiance	Often not available; sensors often covered by snow or rime (Matsui et al. 2012); moisture on radiometer dome.	Calculate potential solar irradiance and estimate transmissivity from diurnal temp. range and vapor pressure (Hungerford 1989; Bristow and Campbell 1984). Attenuation by clouds difficult to model (Male and Granger 1981).	Clear-sky irradiance calculated based on topography (Dozier and Frew 1990), scaled by point measurement or estimate of decrease due to cloud cover	Temporal representation of cloud cover and total atmosphere moisture content (attenuation), consistent with modeled meteorology.
Downward long-wave (LW) irradiance	Often not available, less expensive instruments may be biased. Errors due to snow cover, frost or moisture on radiometer dome (Malek 2008).	Calculated based on surface temperature and vapor pressure or just one of these (Brunt 1932; Brutsaert 1975; Satterlund 1979).	Varies with local air temperature, sometimes LW radiation from surrounding pixels incorporated (Marks and Dozier 1992).	Vertical representation of total atmospheric temperature and moisture can be used to calculate LW irradiance

Finally, in Case 3 an atmospheric model generates surface temperature and precipitation at grid points within a basin, but irradiance is empirically estimated at each point based on the diurnal temperature range and relative humidity of the atmospheric model (e.g., Dettinger et al. 2011; Das et al. 2011). Using an empirical model as the source of irradiance input may be preferable due to biases in atmospheric models stemming from grid size restrictions (Ruiz-Arias et al. 2011) and representation of cloud cover (Edwards and Slingo 1996). However, it is not clear whether empirical models that have been fitted to observed diurnal temperature range and relative humidity will perform as well with atmospheric model input that may be characteristically different from in situ observations.

For each case of meteorological forcing data, we ask the following questions:

1. **How do simulated meteorological variables compare with in-situ observations, particularly in high elevation areas where stations are typically unavailable?**
2. **How and where does the source of forcing data impact simulations of snowpack?**
3. **How does the choice of forcing data impact streamflow simulations in basins draining different elevation ranges?**

To answer these questions we selected the North Fork of the American River Basin (NF American Basin, Figure 1) as a case study. The basin is particularly well suited for exploring the hydrological sensitivity to the choice of meteorological forcings for several reasons. First, it is a relatively simple basin in terms of subsurface contributions: shallow soils, steep topography and negligible ground water contribution during the cool season mean that accurate simulation of streamflow is largely dependent on the meteorological forcing. Second, the National Oceanic and Atmospheric Administration's Hydrometeorological Testbed (NOAA/HMT) program maintains a

dense network of meteorological stations that cover the basin (Ralph et al. 2005). Third, the upper portions of the basin are largely unaffected by water management (such as dams or diversions for water supply), and observations of snowpack and streamflow are also available for the basin.

We use the HMT network and other observational datasets (described in Section 2) to evaluate different cases of empirical and mesoscale input data. In Section 3 we outline specific cases of meteorological sources and use them to determine where they have the greatest impact on simulated snowpack and streamflow using the Distributed Hydrology Soil and Vegetation Model (DHSVM, Wigmosta et al. 1994). Results are reported in Section 4, a brief discussion is provided in Section 5, and conclusions are summarized in Section 6.

Chapter 1

OBSERVED DATA

Our first question was addressed by comparing all suitable meteorological observations within the NF American Basin. Locations of all meteorological stations used in this study are shown in Figure 1a and listed in Appendix A. Because 98% of the NF American Basin precipitation occurred from October through June (National Climatic Data Center http://www.ncdc.noaa.gov/oa/ncdc.html), we restricted our analysis to these months. Hourly observations of precipitation and air temperature for water years 2001-2010 (October – September) were obtained from 8 weather stations operated by the California Department of Water Resources (CDWR, data available through the California Data Exchange Center, http://cdec.water.ca.gov/). Measurements of precipitation, temperature, and relative humidity taken every two minutes were obtained at 13 HMT stations in or near the study basin (data available at http://hmt.noaa.gov/). Three stations (Desert Research Institute; HMT) provided downward short-wave irradiance measurements, and three HMT stations observed net-irradiance from 2006 – 2010 (Figure 1a). In addition, 52 self-recording sensors (iButtons) were distributed in trees across the basin (following methods in Lundquist and Huggett 2008) to provide temperature and relative humidity data from 2008-2010.

Continuous daily streamflow measurements at the basin outlet were acquired from the U.S. Geological Survey (Station #11427000, North Fork Dam). In order to allow verification of the simulated internal basin streamflow timing, additional stream stage data (described by Lundquist et al. 2009) for water years 2007 to 2010 were measured in 2 subbasins shown in Figure 1c.

Snow water equivalent data (SWE) were obtained from 6 snow pillows from the CDWR and 2 snowpillows from the U.S. Natural Resources Conservation Service's SNOTEL network (data available at http://www.wcc.nrcs.usda.gov/snow/) (Figure 1c). Four of the snowpillows are located near the basin's climatological snow line at 1500 m (Mizukami and Smith 2012; Shamir and Georgakakos 2006), and four are located above 2000 m.

All data were closely quality controlled for unrealistic outliers, constant values and extreme jumps, following Meek and Hatfield (1994). The two-minute precipitation, temperature and vapor pressure measurements from HMT were aggregated to hourly values if at least 75% of that hour was available; otherwise the hour was considered missing. The temperature data from the self-recording sensors required minor filling to prevent a cold bias when sensors became briefly snow covered (See Appendix B for details). Due to the limited measurement of wind speed at all stations, no correction for precipitation gauge undercatch was attempted (Sevruk 1983).

Chapter 2

METHODS

We created three cases of forcing data sources which are the NF American Basin specific counterparts to the general cases described in Table 1. The source of the variables in each case is shown in Table 3, and the methods used to generate them are described below. For each source,

Table 3 Cases of meteorological variable sources used to force DHSVM. For all sources, wind speed was taken from the Secret Town station. Empirical estimates are based on the diurnal temperature range (DTR) and the relative humidity (RH).

Variable Source/ Case description	Precipitation, Temperature, Relative humidity	Short-wave Irradiance	Long-wave Irradiance
Case 1: "Secret town station+ Empirical"	Observations from Secret Town (SRT) station	Empirical estimation (Thornton and Running 1999) using: • DTR from SRT station • RH from Tmin=Tdew assumption (Running et al. 1987)	Empirical estimation (Dilley and O'Brien 1998) using: • DTR from SRT station • RH from SRT station
Case 2: "ALL WRF"	WRF model output	WRF model output	WRF model output
Case 3A: "Empirical SW with RH from the Tdew assumption"	WRF model output	Empirical estimation (Thornton and Running 1999) using: • DTR from WRF • RH from Tmin=Tdew assumption (Running et al. 1987)	WRF model output
Case 3B: "Empirical LW with RH from the WRF model"	WRF model output	WRF model output	Empirical estimation (Dilley and O'Brien 1998) using: • DTR from WRF model output • RH from WRF model output
Case 3C: "Empirical LW with RH from the Tdew assumption"	WRF model output	WRF model output	Empirical estimation (Dilley and O'Brien 1998) using: • DTR from WRF model output • RH from Tmin=Tdew assumption (Running et al. 1987)

we compared wet season (defined as October-June) averages of distributed temperature, relative humidity and accumulated precipitation to observations. Comparing elevational gradients of relative humidity is problematic as it includes temperature errors; therefore, all relative humidity measurements and estimations were converted to vapor pressure for comparison. Estimated short- and long-wave irradiance data were separated into clear and cloudy days using a clear sky index based on the observed daily short-wave irradiance. Daily averaged values greater than half of the maximum clear sky irradiance were defined as clear. Modeled streamflow from DHSVM was evaluated using the percent bias of flow and the Nash-Sutcliff efficiency.

a) Case 1: Limited Observations

A common constraint for hydrological studies within complex terrain is to have only one available observational station measuring maximum and minimum temperature, and daily accumulated precipitation at low to middle elevations. The relative humidity, and short- and long-wave irradiance inputs required by distributed hydrological models must then be estimated at the station, and all variables distributed to the rest of the basin. We simulated this type of observationally-based forcing set by selecting the Secret Town station (Figure 1a) as our base station. This station was selected because it is located below the snow line at 829 m, which allowed easier maintenance and resulted in minimal missing data over the 2001 to 2010 period of interest (0.5% missing precipitation data, 1% missing temperature data).

Following the methods of Thornton and Running (1999), the potential daily short-wave irradiance and its transmissivity through the atmosphere were calculated at the Secret Town station based on the observed diurnal temperature range and daily relative humidity, which itself was estimated by assuming that saturation occurred during the daily minimum air temperature. Daily values of short-wave irradiance were then disaggregated to a 3-hourly time-step according

to the local solar zenith angle. Following the recommendations of Flerchinger et al. (2009) we used the algorithm of (Dilley and O'Brien 1998) to estimate mean daily downward clear sky long-wave irradiance from the diurnal temperature range and daily relative humidity. Adjustments for cloudy sky were made following (Marks et al. 1998) using estimates of precipitable water from Prata (1996). We note that there exists variability among empirical irradiance models, although we focus only on the above selections for brevity.

Next, each variable was extrapolated from Secret Town to a 150 m grid over the NF American Basin. Precipitation was distributed using the spatial weighting from a 30 arc second (800 m) 1971-2000 climatological normals product, derived using the Parameter Regression on Independent Slopes Model (PRISM, Daly et al. 1994, 2004). The temperature record from the Secret Town station was extrapolated using an average annual lapse rate of -6.5 °C km^{-1}, based on California climatology (Daly et al. 2008). Vapor pressure was extrapolated using a -1.25 °C km^{-1} dew point lapse rate (Franklin 1983). Solar shading was accounted for by splitting the downward short-wave irradiance into diffuse and direct components, which were corrected using monthly maps of terrain shading based on solar geometry and a 150 m digital elevation model (Wigmosta et al. 1994). Long-wave irradiance was distributed uniformly across the basin.

b) Case 2: Output from the WRF model

We selected as a mesocale model, the Weather Research and Forecast model (WRF, Skamarock and Klemp 2008) to generate 6 km surface meteorological data for 10 partial water years (October-June of water years 2001-2010). Boundary conditions were provided by the North American Regional Reanalysis (NARR), a 32 km gridded product created by ingesting surface and upper air observations over the continental U.S. (Mesinger et al. 2006). In order to allow the surface output of the WRF model to be comparable to the historic observations, we

reinitialized its boundary conditions every 5 days with 3 hours of spin up, resulting in a temporally continuous simulation. This technique takes advantage of the accurate forecasting range of the WRF model (~5days) and has been shown to capture the variability in meteorological conditions over an 11-year period in Southern California when generated with the Penn State/NCAR mesoscale model (MM5), version 5, WRF's predecessor (Hughes and Hall 2009). For complete details of the WRF model configuration and downscaling methods see Dettinger et al. (2011). Note that the Morrison 2-moment microphysics (Morrison et al. 2009) is used here.

Surface output from 61 of the WRF model's 6 km grid cells across the NF American Basin and at 8 nearby snowpillow locations was extracted (Figure 1a and 1b). At each grid cell, hourly precipitation, 2-meter temperature, 2-meter water vapor mixing ratio and downward short- and long-wave irradiance were extracted from the WRF model for the wet season of water years 2001-2010. Relative humidity and vapor pressure were calculated from the water vapor mixing ratio, temperature and pressure. The center of each 6 km grid cell was treated as a pseudo station, and each meteorological variable was interpolated to a 150 m grid using inverse distance weighting. Differences between the 6 km and 150 m grid elevations were accounted for by adjusting temperature according to the local observed annual average lapse rate of -6.5°C km^{-1}. Due to the relatively small contribution from turbulent fluxes to the snow energy balance (Marks and Dozier 1992), we did not focus on the WRF model's wind speed, but instead followed the assumption of previous studies and uniformly distributed the observed wind speed from the Secret Town station (Waichler and Wigmosta 2003). The comparison between the forcing data in Case 1 and 2 (Section 4) highlights which variables improved from using the more computationally expensive WRF model to produce the meteorological forcing data.

Case 3: Combination of the WRF and empirical models

This case of meteorological data emulates those studies that used temperature, precipitation and relative humidity from mesoscale model output, and then estimated short- and long-wave irradiance using empirical models (Case 3). Temperature and precipitation were used as in Case 2 from the WRF model, and short- and long-wave irradiance were estimated at these points using the empirical methods described in Case 1. In addition, we created variants on Case 3 in order to independently test the impact of different relative humidity sources on empirical estimation of short- and long-wave irradiance. Case 3A empirically estimated short-wave irradiance using relative humidity based on the dew point assumption, and WRF model long-wave irradiance. We compared Case 3A and Case 2 to illustrate the different characteristics of downward short-wave irradiance estimation between an empirical model and the WRF model.

In Case 3B and 3C we empirically estimated long-wave irradiance based on relative humidity data from the WRF model and from the dew point assumption, respectively. Both Case 3B and 3C used the WRF model short-wave irradiance. The comparison between Case 3B and 3C will determine the importance of accurate relative humidity data for empirical estimation of long-wave forcing data. These last two variants of Case 3 will then be compared to the WRF model (Case 2) and observations in order to identify how, and within which locations, errors from different sources of long-wave irradiance most impact simulated snowpack and streamflow.

c) Hydrological simulations of the NF American Basin

To evaluate the impact of simulated hydrologic variables, each meteorological forcing set in Table 3 was then used to drive the Distributed Hydrology Soil and Vegetation Model, DHSVM, which is a fully distributed, physically based hydrological model that simulates the surface energy and water balance and the transport of water as a function of meteorological

forcing, topography, soil drainage characteristics, and vegetation cover (Wigmosta et al. 1994; Waichler and Wigmosta 2003). It has commonly been applied at grid scales ranging from 30 to 180 m over basins that include complex terrain (Leung et al. 1996; Westrick 2001; Westrick and Storck 2002; Zhao 2009, and Nijssen et al. 1997). For each time step at each grid cell, DHSVM uses a full energy balance approach to determine snow accumulation and ablation within the overstory and understory (if present) and at the surface (Andreadis et al. 2009). Surface and subsurface moisture transport are simulated via the topographic gradients between grid cells, with water ultimately propogating to the simulated stream network, where a 1-dimentional routing scheme is used to calculate streamflow at the basin outlet (Wigmosta et al. 1994).

DHSVM was set up to run at a 150m grid resolution and 3-hour time step over the NF American Basin (Figure 1a) and in point mode at selected snowpillow stations (Figure 1c). This grid cell size was chosen to balance the need to accurately represent the North Fork basin's topography with computational expense. Soil type and land cover data were obtained from the STATSGO and USGS databases (Soil Survey Staff 2006, U.S. Geological Survey 2005). The basin is predominantly covered by evergreen needle leaf (71%), as well as open shrub (17%) and mixed forest (6%). At every time step and at each grid cell, DHSVM requires the following meteorological forcing data: precipitation, temperature, vapor pressure, wind speed, and downward short- and long-wave irradiance.

A full model calibration of DHSVM for the NF American basin was beyond the scope of our investigation and instead standard parameters were chosen based on previous studies (Wigmosta et al. 1994, Storck 2000). Model performance as it relates to our specific use of the model in the experiments is evaluated in subsequent sections.

Chapter 3

RESULTS

a. How do different sources of precipitation compare?

Wet season accumulated precipitation values from Case 1 (one measurement site extrapolated using PRISM climatology) and Case 2 (WRF output) are plotted against elevation and compared to observations in Figure 2. For most years, the PRISM forcing (Case 1) and the WRF model (Case 2) capture the correct averaged orographic precipitation gradient; yet some years, such as 2002 and 2003, show large biases. For example, the WRF model has a 234 mm (26%) and 458 mm (34 %) wet bias during water years 2001 and 2003, while the PRISM-based estimates more closely match observations. In contrast, the PRISM-based estimations had a 237.0 mm (-18.2%) dry bias in 2002, while WRF more closely matched observations. Also, during water year 2006, when the study domain received 180% of the climatological average, the PRISM forcing (Case 1) overestimated precipitation observations by 409 mm (17.2%), while the WRF model (Case 2) had a -68 mm (-2.9%) bias. These errors are related to the relationship between the PRISM base station (Secret Town, the lowest elevation green dot in Figure 2) and the higher elevation stations. During years when the Secret Town station measured more or less precipitation relative to the surrounding stations, Case 1 errors were large. Averaged over the entire study period, the WRF model had a consistent bias of +196 mm (17%), although some of this difference is likely due to gage undercatch, which was not accounted for in the observations.

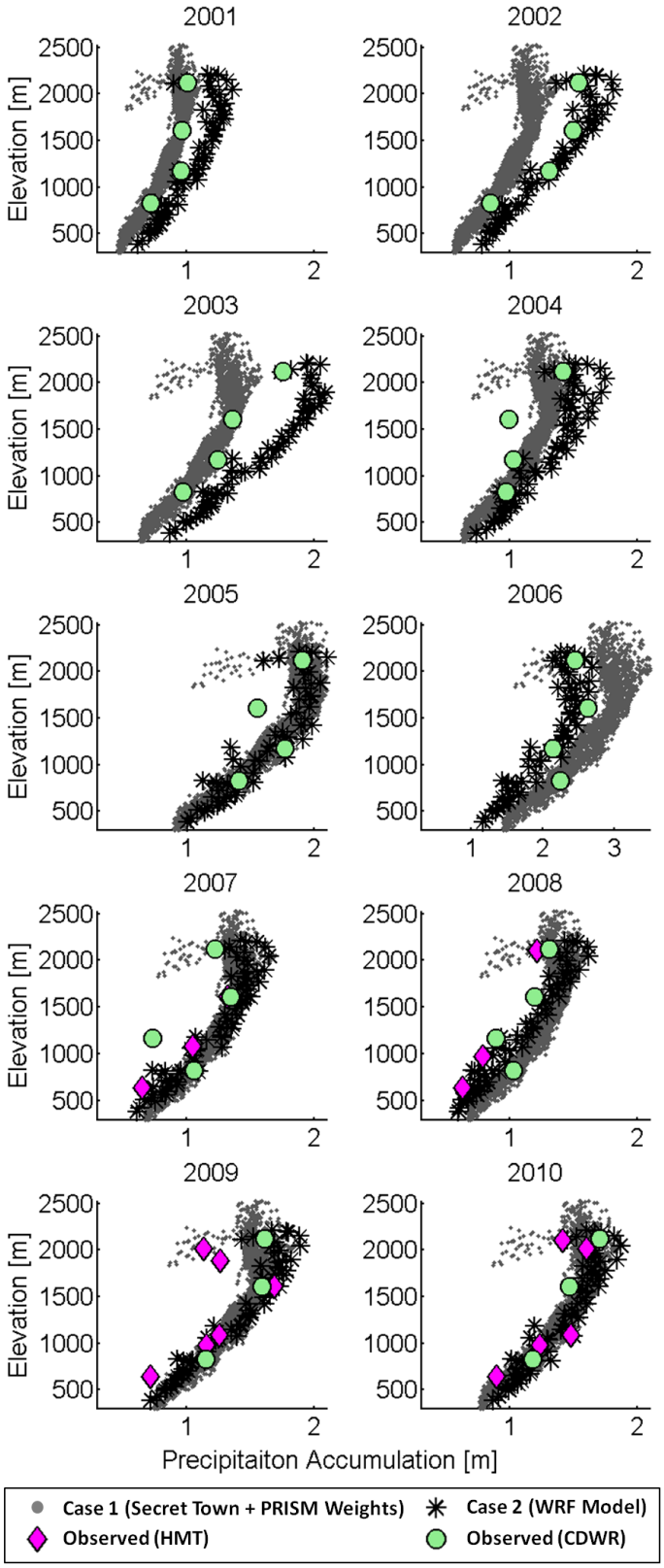

Figure 2 Total wet season accumulated precipitation versus elevation for water years 2001 through 2010. *Black stars* show the WRF model precipitation for each of the (61) 6km grid cells. The *grey dots* represent the observed precipitation at the Secret Town station extrapolated using weights from PRISM climatology (see section 3 for details). Observations from HMT and CDWR stations are shown as *pink diamonds* and *green circles*, respectively. Note: Water year 2006 required a different x-axis scaling.

b. Impact of precipitation forcings on simulations of streamflow

Over the 2001 to 2010 period, the DHSVM modeled streamflow had adequate performance when compared to daily observations at the basin outlet. For the entire study period, Case 1 and Case 2 had daily Nash-Sutcliffe efficiency (NSE) values of 0.57 and 0.53, and percent biases of -3.4% and 0.8%, respectively. The poor NSE values are likely the result of the uncalibrated model and the period of statistics considered, October through June, which include more variable streamflow than the summer months not examined here. While the percent biases were low over the entire period, individual years had larger biases depending on the source of precipitation forcing.

Years when the source of precipitation was biased low/high, resulted in biased low/high simulated total streamflow. Two example years, 2003 (Figure 3) and 2006 (Figure 4) highlight how biases in precipitation propagate into simulated streamflow. During 2003, Case 1 (the Secret Town station and PRISM) had a -102 mm (-7.7%) accumulated precipitation bias, while Case 2 (The WRF model) had a +457 mm (+30.3%) bias (Figure 1). Simulated streamflow from both cases at the basin outlet during 2003 is shown in Figure 3a. The largest simulated streamflow errors occurred at the end of December and early January (Figure 3b), leading to biases in the total accumulated streamflow (expressed in basin equivalent precip) of -349 mm (-47.5%) in Case 1 and +144 mm (19.6%) in Case 2 (Figure 3c).

In contrast, during water year 2006 (Figure 4) the biases in precipitation forcings (and resulting simulated streamflow bias) had opposite signs as 2003. Case 1 had a precipitation bias of +409 mm (17%) and resulting total streamflow bias of +403 mm (26%), while Case 2 had a precipitation bias of -68 mm (-3%) and a total streamflow bias -252 mm (-16%). These two

examples illustrate the importance of selecting an accurate source of precipitation forcing for unbiased simulation of streamflow. However, because the timing of simulated streamflow is also dependent on simulated snowpack and other meteorological forcing variables, we examine these impacts below.

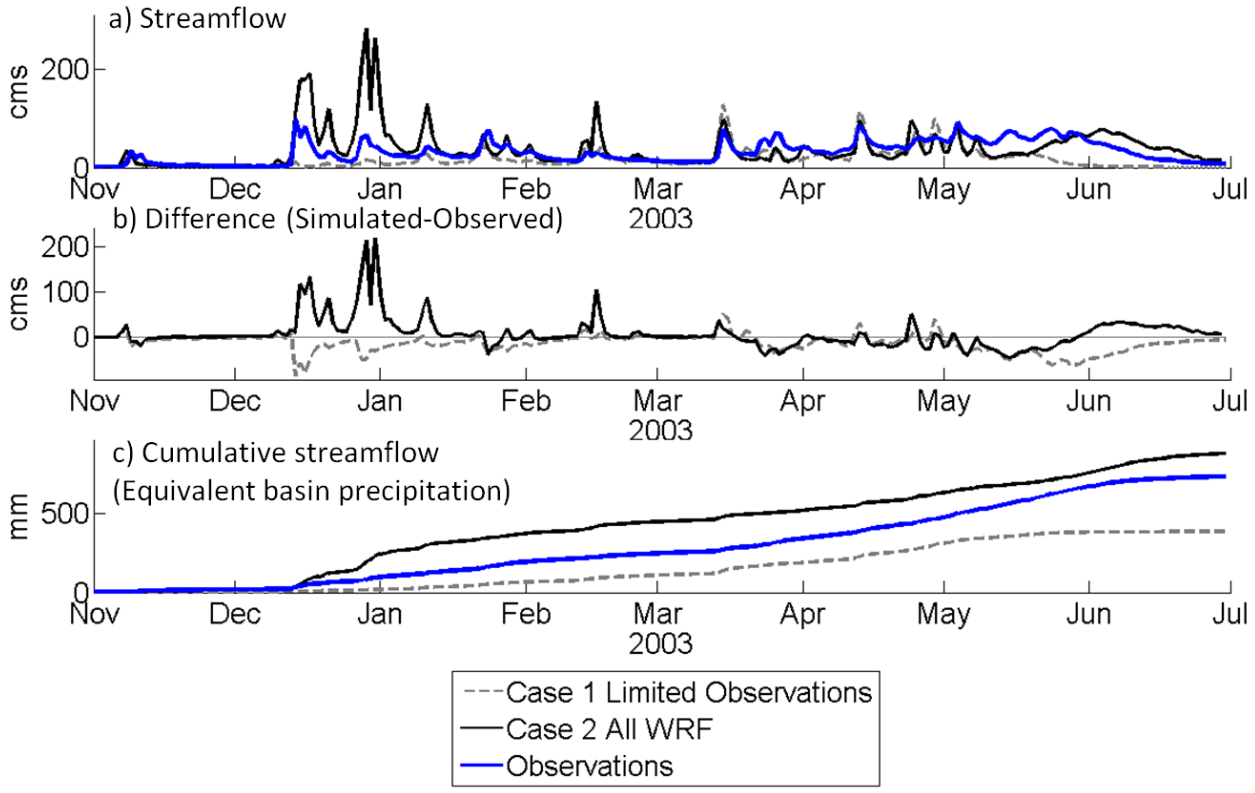

Figure 3 a) DHSVM's modeled streamflow at the NF American Basin outlet and b) error compared to observations at the NF USGS gauge for water year 2003. The cumulative streamflow expressed as equivalent basin precipitation is shown in c).

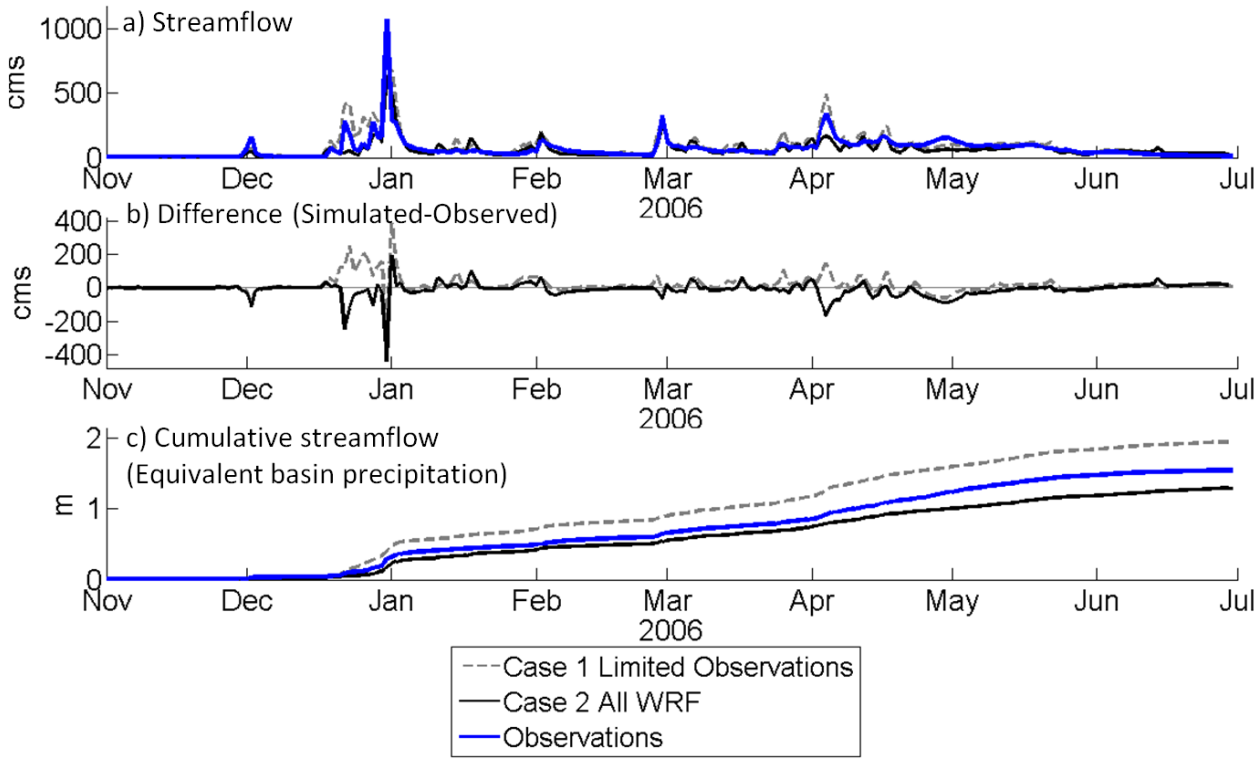

Figure 4 Same as Figure 3, but for water year 2006.

c. How do different sources of temperature compare?

The two sources of estimated temperature agreed well with observations of mean temperature and with each other over all water years. Figure 5a shows the mean wet season mean temperature plotted against elevation for water years 2008 to 2010 when additional HMT, CDWR, and iButton records were available for comparison. The WRF model output was not statistically different from the temperatures estimated using the simpler Case 1 method during the averaged wet season period. However, on sub-daily time scales, the two sources of temperature had different averaged diurnal temperature ranges (Figure 5b). The WRF model's diurnal temperature range (Case 2) was on average 3.0°C lower than the average of all observations sites, while Case 1 was on average 2.6°C larger. Interestingly, the differences between these two estimated forcings was as large as the variance between observations. In

regards to hydrological modeling, errors/accuracy in the diurnal temperature range are important because they can bias empirical estimates of short-wave irradiance and simulations of transpiration.

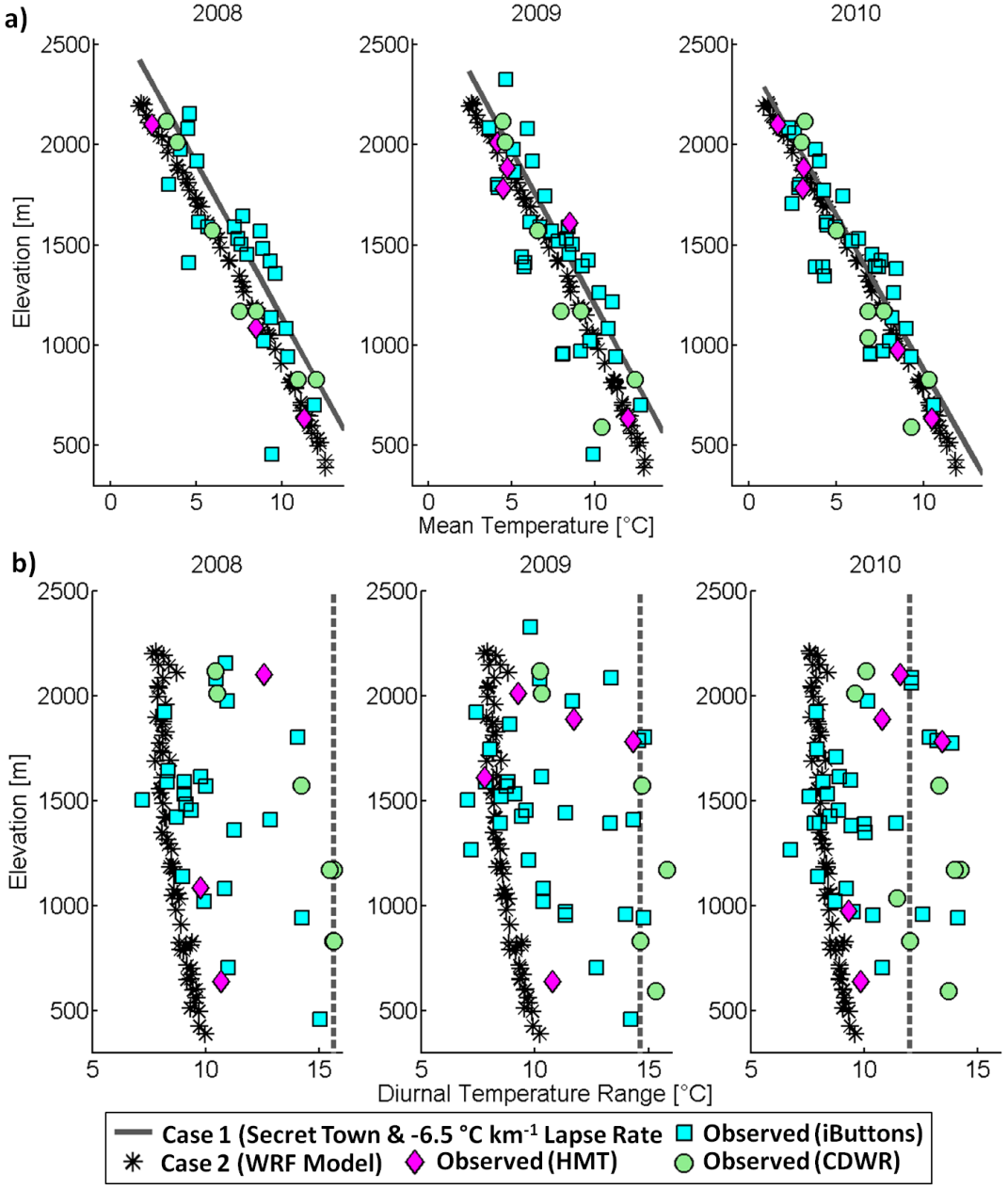

Figure 5 a) Mean Oct-June air temperature versus elevation for water years 2008 to 2010. b) Averaged diurnal range of temperature from Oct. to June for water years 2008-2010. Dashed line indicates constant diurnal temperature range resulting from lapsing temperature from the Secret Town station.

d. How do different estimates of vapor pressure compare?

Empirical models of long-wave irradiance are dependent on the surface vapor pressure to provide an estimate of cloudiness and of atmospheric transmissivity during clear sky conditions (Kimball et al. 1982); therefore, three sources of estimated surface vapor pressure were compared to observations (Figure 6). For Case 1, the assumed -1.25 degree C km^{-1} dewpoint lapse rate (proposed by Franklin (1983) and used in Running et al. 1987) from the Secret Town station did not match the decreasing gradient of observed vapor pressure over the NF American Basin. The WRF model (Case 2) generally captured the observed gradient of vapor pressure, yet had a mean bias overall of -190 Pa across all elevations. When we used the WRF model's minimum air temperature to estimate the dew point, the resulting average vapor pressure (Case 3C) had a mean bias overall of +245 Pa. For comparison, the averaged difference between Case 2 and Case 3C in terms of relative humidity is 31.9%.

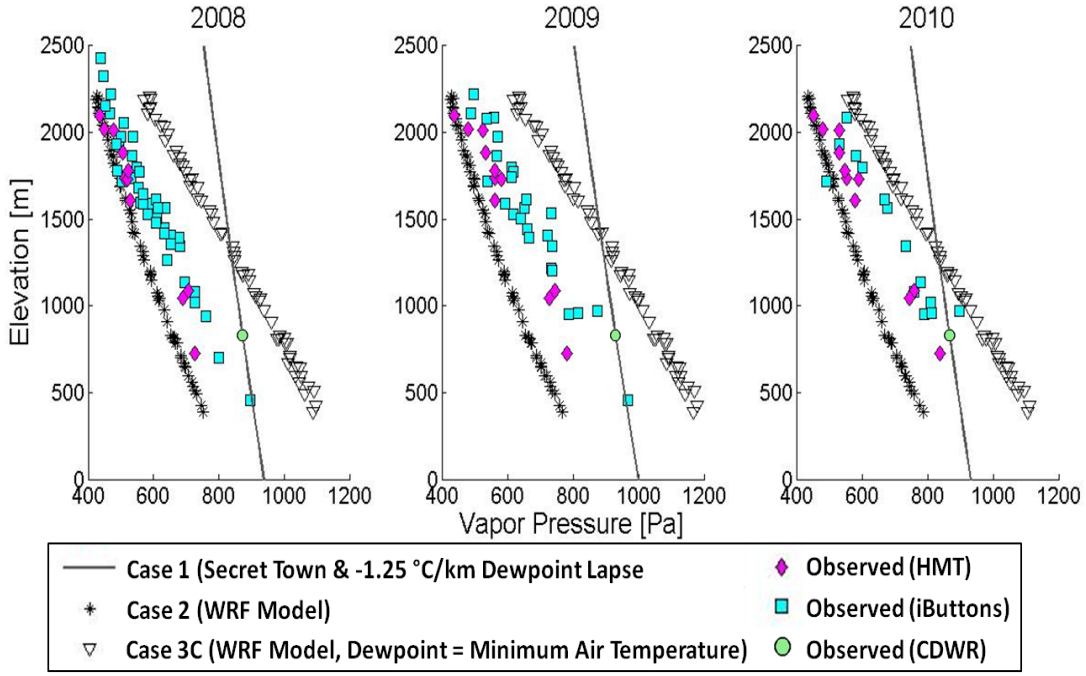

Figure 6 Average Oct–June vapor pressure versus elevation for water years 2008-2010, within the region of the North Fork Basin. All relative humidity measurements and observations were converted to vapor pressure.

e. Comparison of estimated irradiance forcing sources

Three stations measured downward short-wave irradiance from 2006 to 2010 (Figure 1a). We examined the mean daily fluxes between March and June to highlight differences in the estimated forcings during the melt season. Comparisons between daily observed fluxes and the estimated forcing sources are shown in Figure 7a for clear days and in Figure 8a for cloudy days (defined in Section 3). On clear days, the effect of topographic shading can be seen in the lower median values of the observe short-wave irradiance at the Sierra Snow Lab and Big Bend stations, and the higher median values at the Foresthill station. The DHSVM shading algorithm accurately captured the differences in median short-wave irradiance between stations for all sources of forcing data. Another interesting result was that the empirical estimation of short-wave irradiance using the radiation directly output from the WRF modeled temperature range (Case 3A) had average median values 37 Wm^{-2} less than the WRF model (Case 2). On cloudy days (Figure 8a), both of the empirical estimates (Cases 1 and 3A) were consistently positive biased, while the WRF model (Case 2) was not statistically different from observations at Big Bend and Foresthill, and was the least biased option at the Sierra Snow Lab. In general, the WRF modeled short-wave irradiance performed better than the empirical models tested.

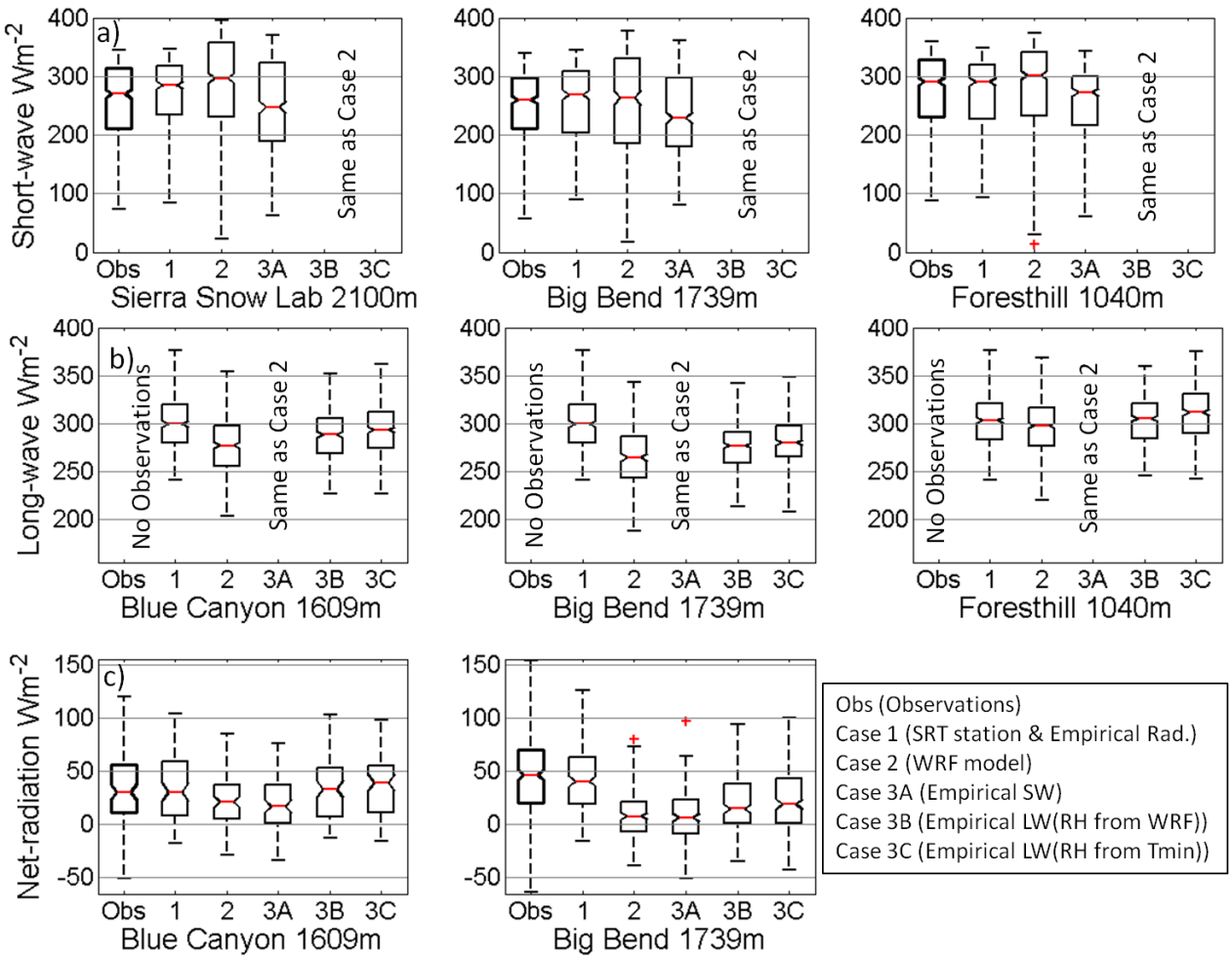

Figure 7 Averaged daily statistics from each radiation forcing over *clear* days between March and June of a) downward short-wave irradiance, b) downward long-wave irradiance and c) simulated net-irradiance compared to available observational stations. X-axis identifies the case number for each model run (see legend), and the columns identify the site location. Note that the left-hand column shows shortwave at the Sierra Snow lab but Longwave and Net radiation at Blue Canyon. We define clear days when the mean observed short-wave irradiance is greater than half of the daily averaged maximum short-wave irradiance. *Red crosses* show outliers.

No direct observations of downward long-wave irradiance were available to test the accuracy of the estimated long-wave forcings. However, substantial differences between sources of estimated long-wave irradiance were found during both clear and cloudy periods (Figure 7b and 8b). The long-wave irradiance from Case 1 was empirically estimated at the Secret Town station and uniformly distributed across the basin, resulting in a median value of 311 Wm^{-2} on cloudy days. In contrast, the long-wave irradiance calculated by the WRF model (Case 2)

decreases with elevation, with median values of 329, 295 and 281 Wm^{-2} at Foresthill (1040m), Blue Canyon (1609m), and Big Bend (1739m), respectively. This behavior is expected based on the observed decrease of surface temperature and vapor pressure in the atmospheric column at higher elevations, resulting in lower long-wave radiance emission (Marty et al. 2002). The median values of Cases 3B and 3C also decreased with increasing elevation, but within a smaller range.

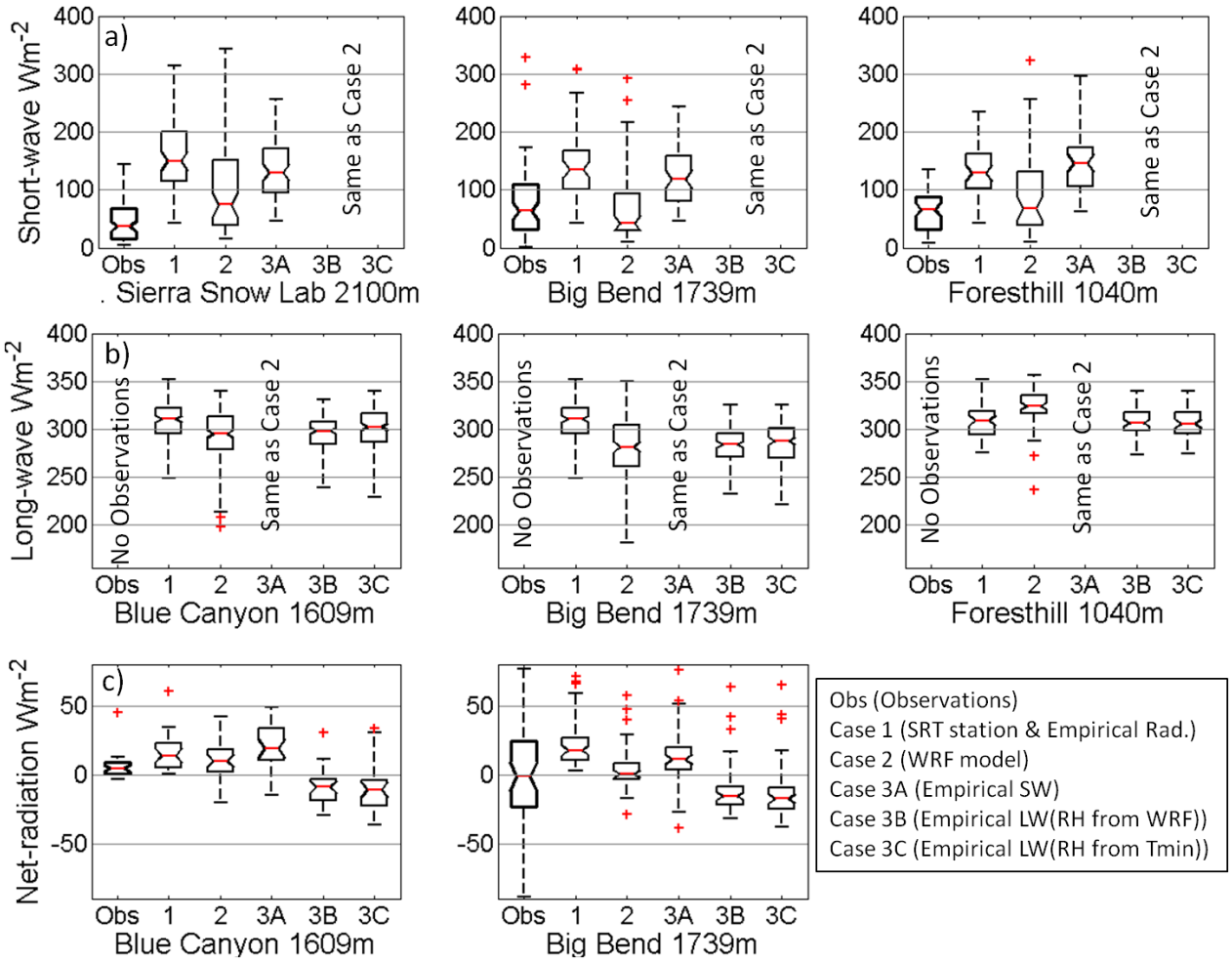

Figure 8 Same as Figure 5, but for *cloudy* days. We define cloudy days when the mean observed short-wave irradiance is less than half of the daily averaged maximum short-wave irradiance.

Each case of irradiance forcing was used to force the DHSVM model over the NF American Basin, and simulated net-irradiance values at the surface were compared to point

observations at the sites shown in Figure 1a. For both clear and cloudy periods, the differences between each source of short- and long-wave forcing propagated into the simulated net irradiance (Figures 7c and 8c). However, the evaluation of net irradiance was complicated by differences in the snow surface albedo, for which no direct observations were available. The simulated albedo decay was parameterized in DHSVM as a function of days since last snowfall (Laramie and Schaake 1972), which was the same for Cases 2, 3A-C, which all had the same precipitation input. During clear days (Figure 7c), the WRF model had larger median biases in net radiation at the higher-elevation station, Big Bend (-39 Wm^{-2}), than at the lower station, Blue Canyon (-9 W m^{-2}). The empirical estimations of long-wave (Case 3B and 3C) resulted in slightly less biased median values of -32 and 3 Wm^{-2}, and -28 and 9 Wm^{-2}, at Big Bend and Blue Canyon, respectively.

f. Impact of long-wave irradiance forcings on simulations of snowpack

Because the differences between estimated long-wave forcings showed the greatest variation during the melt season (Figure 7a), we examine the impact of this variable on simulating snow melt. Two snow observing stations were selected to illustrate the impacts of estimated forcings at high (Sierra Snow Lab, 2100m) and middle (Blue Canyon, 1609m) elevation sites. Figure 9a shows observed and simulated SWE at the Sierra Snow Lab (2100m) for each different long-wave forcing case over water year 2009. All other forcing variables were taken from WRF and were constant between simulations. SWE simulated at the high elevation site (Sierra Snow Lab) only differed between Cases 2, 3B and 3C after March when the

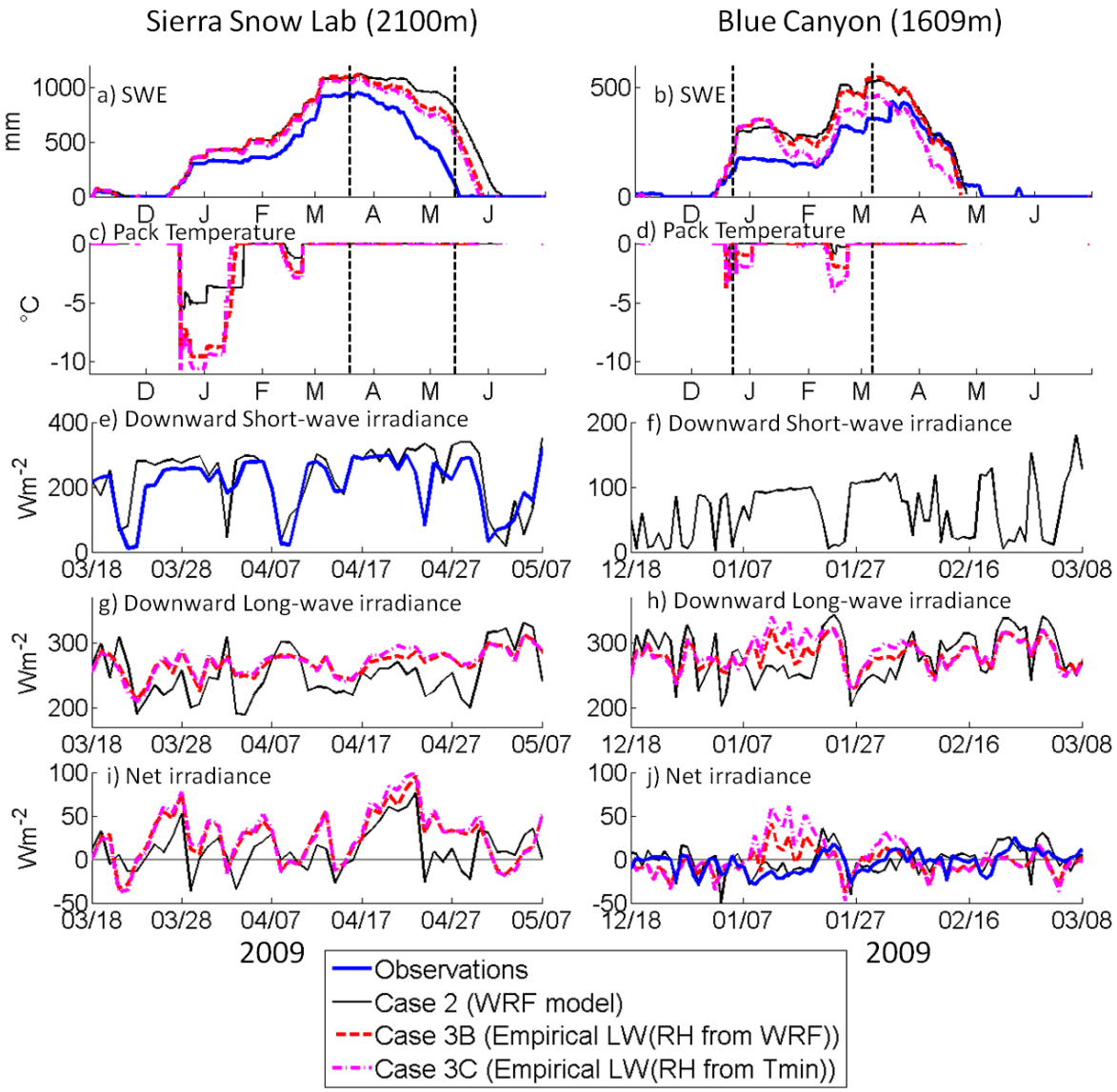

Figure 9 (a,b) Simulated SWE from DHSVM compared to observations at the Sierra Snow Lab (2100m) and Blue Canyon (1609m) during 2008 – 2009. Modeled (c,d) internal pack temperature, (e,f) downward short-wave irradiance, (g,h) downward long-wave irradiance, and (i,k) net-irradiance. Note that the timeperiod of plots e,g,i focus on the melt season (March-May), and plots f,h,j focus on the erroneous mid-winter melt event during January – time-periods marked with vertical dashed lines in (a) and (b).

simulated pack temperature increased to the melting point (Figure 9c). During this period, the differences in simulated net-irradiance (Figure 9i) between the WRF model (Case 2) and the empirical forcings (Case 3B and 3C) result in different simulated melt rates. Case 2 had the lowest simulated melt rats and the lowest net-irradiance, which was consistent with the negative bias found in the WRF model net irradiance (Figure 7c). The difference in long-wave forcings

between Case 3C and Case 2 resulted in the simulated snow disappearance date at the Sierra Snow Lab station to shift later by 12 days, which was consistent with a shift towards later snow disappearance during other years (not shown). Empirical estimates of LW (Cases 3B and 3C) were relatively insensitive to the source of RH during this spring melt period (Figure 9 a, g, i).

In contrast, the simulated snowpack at the Blue Canyon station (Figure 9b) at a lower elevation of 1609 m, had a warmer pack temperature throughout the winter (Figure 9d) and thus was more sensitive to winter biases in the surface energy balance. During a 10-day period in January, the empirically estimated net-irradiance forcings (Figure 9j) were biased high by ~50 Wm^{-2}, resulting in high simulated melt rates that were not observed at the Blue Canyon snowpillow (Figure 9b). This bias in mid-winter melt was largest for Case 3C (empirical LW with RH estimated from T_{min}), and resulted in an offset in simulated SWE for the rest of the season. These January LW irradiance estimates (Figure 9h) were very sensitive to the source of RH, whereas the spring irradiance estimates (Figure 9g) were not.

This example illustrates how simulated snowpack at middle elevation sites are more sensitive to biased irradiance forcings during the winter, whereas higher and colder snowpacks are only sensitive during the spring melt period. To test the robustness of this observation, we compared modeled with observed SWE at 8 snow pillows in the area, 4 above 2000 m and 4 below (Figure 10). For snow in clearings, the January melt bias in Case 3C (empirical LW) was present at all of the lower-elevation snow pillows (in *red*, Figure 10 a,b,c).

While the above biases in long-wave irradiance forcings were shown to have a critical effect on the simulated melt rates at open sites typical of snowpillows, their impact under a forest canopy would be expected to be significantly less, as a higher fraction of long-wave emission comes from the canopy instead of the atmosphere (Pomeroy et al. 2009). Within DHSVM, this

process is parameterized based on the fractional coverage of the vegetation (See Appendix C for a full description), which was set at 0.75 for the 77% of the NF American Basin covered by an overstory canopy (U.S. Geological Survey 2005). Therefore, we evaluate how the presence of an overstory modifies the impact of different long-wave sources on simulated melt rates. As discussed above, simulated SWE within clearings (Figure 10b and 10c) at lower elevation sites (*red)* showed strong sensitivity to the lower long-wave forcing of Case 2. However, the same forcings applied under a canopy with 0.75 fractional coverage reduced the difference between the simulations in Case 2 and Case 3C. At lower elevations, the simulated snow under the forest canopy melted in January regardless of how atmospheric long-wave irradiance was prescribed. Thus, within forested regions, the source of long-wave irradiance appears to be less important than the correct modeling of the canopy temperature. Because we do not have SWE measurements under the canopy, this remains an area for future investigation.

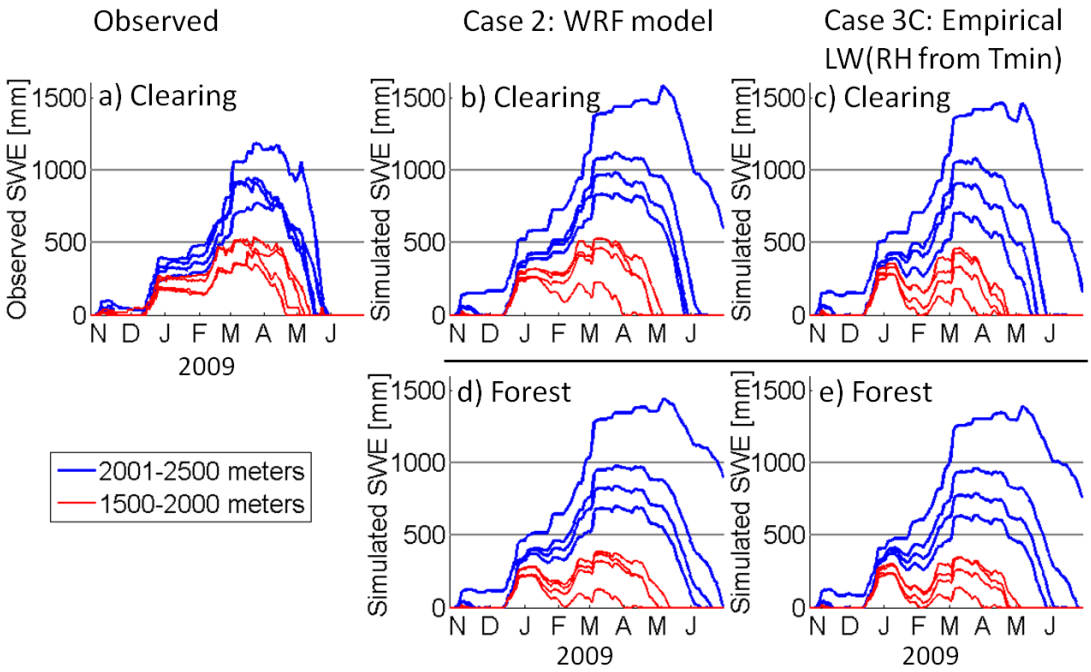

Figure 10 a) Observed SWE during the 2008-2009 period at the 8 snowpillows in or surrounding the NF American Basin, separated into stations above and below 2000 meters elevation. Point simulations of SWE with forcings from Case 2 and 3C are shown for b,c) no vegetation (bare soil resembling a snowpillow) and

d,e) a forest overstory with 0.75 fractional coverage (representing the vegetation type covering 77% of the NF American Basin).

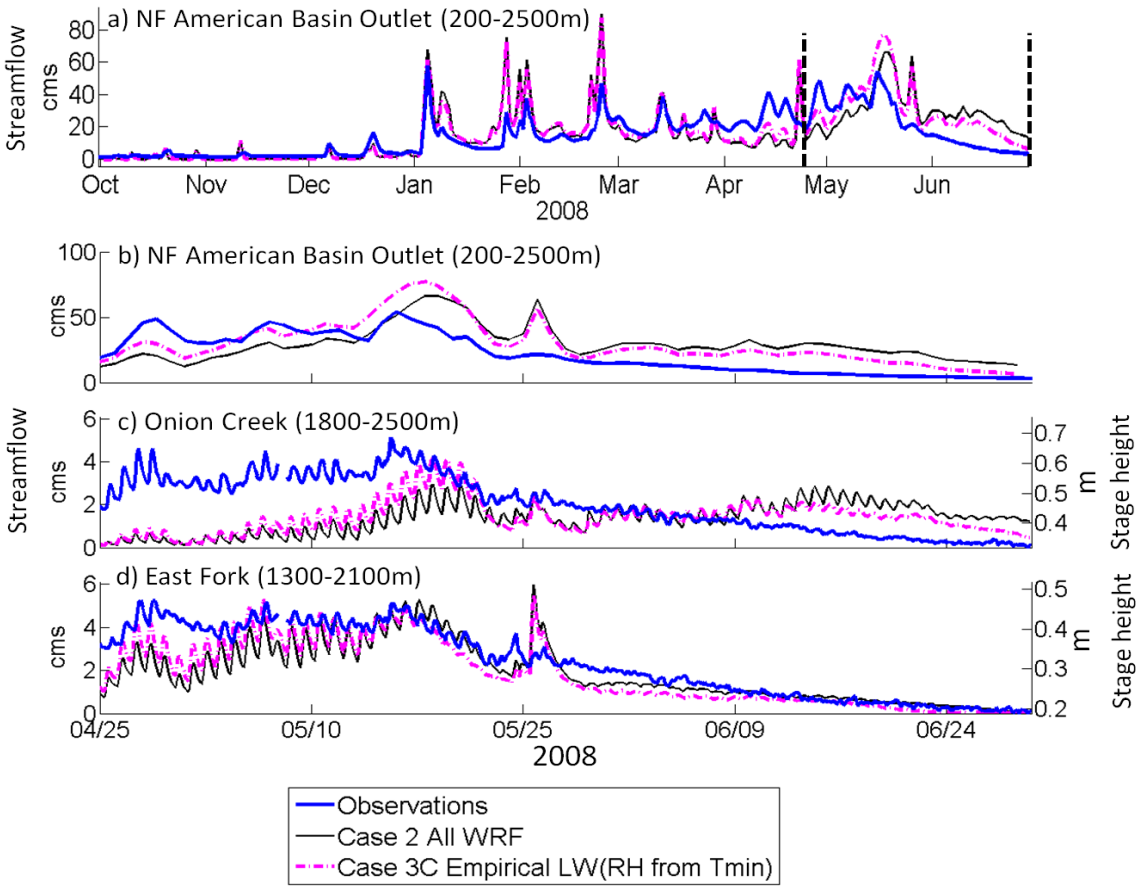

Figure 11 DHSVM's modeled daily streamflow at a) the NF American Basin outlet compared to daily observations at the NF USGS gauge for water year 2008. Dashed lines identify the period shown with a zoomed in view in b, c, and d). Simulated 3-hourly streamflow at, c) Onion Creek and d) East Fork sub-basins compared to 3-hourly observed stream stage (*right axis)*. Note, c) and d) only compare timing of streamflow.

g. Impact of long-wave irradiance forcings on timing of simulations of streamflow

Figure 11a shows modeled streamflow at the NF American Basin outlet compared to observations for 2008. Empirical LW forcing (Case 3) resulted in faster spring melt, which is illustrated by more flow in May and less flow in June than the all-WRF forcing scenario (Case 2). The impact on basin aggregated streamflow from different long-wave irradiance forcings was not as significant as one might expect from the snow pillow simulations due to the high forest density over the NF American Basin. Both simulations of streamflow had the largest errors

during individual storms, and during the melt season (Figure 11b). At each sub-basin (Figure 11c and 11d), the observed stage height featured diurnal snowmelt cycles through mid-May and then decayed throughout June. Both simulations of streamflow captured this pattern at the lower East Fork Basin, but both have prolonged snowmelt and higher streamflow throughout June at the higher Onion Creek Basin. These simulated streamflow errors at the higher sub-basin propagate into the basin outlet (Figure 11b). In general, neither long-wave forcing case was found to explain low spring melt rates and errors in simulated streamflow timing over the NF American Basin.

Chapter 4

DISSCUSION

The meteorological forcings from the 6km WRF model compared to in-situ observations were found to perform as well as, or better than, other sources examined in this study. This is a particularly important finding because such models can be produced in areas with limited station coverage, or even in remote areas that do not have any access to any other sources of data. That said, it is important to note that the WRF model was configured to produce a "best case" forcing data scenario, using updates from a reanalysis product every five days to prevent the large-scale weather systems from diverging from the historical observations. Data assimilation incorporated in the large-scale forcing used to drive the WRF simulations (and in particular accurate vertical soundings from nearby meteorological stations) would not be present in remote areas where inaccuracies in the large-scale forcing would be expected to degrade performance. For similar reasons, degradation of the accuracy of the WRF model output is likely to occur when a free running global circulation model is used instead of a reanalysis product (e.g. in climate change assessments). In addition, the transferability of these results to other regions may be dependent on the configuration of the WRF model. For example, the choice of the microphysics scheme and representation of cloud cover can affect the short- and long-wave irradiance at the surface (Edwards and Slingo 1996). However, for this configuration of the WRF model, we found that the short-wave irradiance performed better than empirical estimations using the WRF model temperature, especially during cloudy days, and therefore recommend the use of short-wave irradiance from the WRF model if available. One possible explanation for this improved performance over other methods is that the physical representation of atmospheric moisture

content led to the improved short-wave irradiance values over the NF American Basin, although further work will be needed to test this hypothesis.,

Biases in the precipitation forcings from the Secret Town station and PRISM weights (Case 1) and the WRF model (Case 2) were found to vary in magnitude and sign between years. Averaged over the entire study period, Case 2 had a consistent positive bias of +196 mm, although water year 2006 did have a negative bias (-68 mm). In contrast, Case 1 did not show a consistent accumulated precipitation bias, under-predicting observed values on average by -123 mm during 2001-2003, and over-predicting by +183 mm from 2004-2010. The variation of the bias in Case 1 is related to the relationship between the PRISM base station and the higher elevation stations, while the consistent bias in Case 2 may be caused by the choice of microphysics scheme, as Chin et al. (2010) suggests in a study over California, or by gage undercatch. These results suggest that if the only available station measuring precipitation is unrepresentative of the basin wide orographic gradient, then the WRF model may provide a more consistent precipitation forcing. Given that in most locations, we have limited means of assessing whether one existing station is representative, WRF is likely a better choice in areas of limited surface observations.

The biases in precipitation forcing for a given year were found to significantly impact the DSHVM simulated streamflow at the NF American Basin outlet. Two examples years were used to illustrate how biased dry and wet precipitation forcings propagated into the total volume of simulated streamflow. Although DHSVM was uncalibrated, because the NF American Basin has steep slopes, shallow soils and little storage, we expect the relative magnitude of the simulated streamflow response to different precipitation biases to remain unchanged following calibration.

In general, no single meteorological forcing set considered here was able to capture the observed melt rates at all elevations and during the entire study period. At higher elevation sites (~2000-2500 m), the simulated melt rates during early spring were lower than observations at snowpillow locations, contributing to a bias in simulated streamflow timing at the higher sub-basin (Onion Creek) and in the aggregated basin output. Simulated snowpacks at mid-elevation sites (~1500-2000 m) were found to be more sensitive to short-term positive biases in the radiation forcing than higher elevation sites. This was illustrated during a warm period in January of 2009, when higher values of empirically estimated long-wave irradiance caused high melt rates that were not observed. The sensitivity of warmer snowpacks in clearings has also been noted by Kuraś et al. (2011, their Figure 4), who found DSHVM simulated melt prematurely in clearings but not under forest canopy, and suggested the cause was the representation of the snow albedo decay. Our results suggest that this bias may, alternatively, be due to errors in estimates of incoming LW irradiance. However, another explanation is that errors in the simulated turbulent energy fluxes, which are on average small or opposite in sign (Marks and Dozier), may have become significant for short periods, yet this remains for future work.

Despite the intensive observations within the NF American Basin (Figure 1a and 1c, and Appendix A), the diagnosis of the biased melt rates was limited by the lack of observations of albedo and upward and downward long-wave irradiance, especially under forest canopy. Short of installing additional stations to provide these measurements, future work will examine different methods used to simulate the albedo decay, snow surface temperature, and internal energy storage.

SUMMARY OF CONCLUSIONS

This study used the Distributed Hydrology Soil and Vegetation Model to examine the impacts of different cases of meteorological forcing data on simulated snowpack and streamflow within the North Fork American River Basin region in the Sierra Nevada, California. Three cases of forcing data were created that represent commonly used configurations of forcing data from observations, empirical and mesocale model sources. The average bias in accumulated precipitation during the wet season from the Secret Town station and PRISM forcings had a mean bias of +91 mm, but varied from -237 to 409 mm between years. The WRF model had a higher mean bias of +196 mm, but with the exception of 2006, was consistently positive biased between years. When DHSVM was forced with the precipitation forcing from the WRF model, simulations of accumulated snowpack and total streamflow were biased high by a similar magnitude as the precipitation forcing for each water year, indicating that the precipitation bias is likely not due to gauge undercatch.

The elevational gradients of annual mean temperature from the WRF model agreed well with the climatological -6.5 °C km^{-1} lapse rate, yet failed to capture the daily diurnal temperature range, which was biased low on average by 3.0 °C. Surface vapor pressure estimated by assuming that saturation occurs during the minimum WRF model temperature performed worse than the output from the WRF model itself. Likewise, the empirical estimation of short-wave irradiance based on the WRF modeled temperature had larger average median errors than the WRF model output. Long-wave irradiance from the WRF model captured the expected decreasing mean values with elevation, but whether a low bias in long-wave irradiance caused

simulated melt rates to be too low over the Sierra Nevada remains for future work with additional observations.

In general, the choice of which case of meteorological forcing was best was not the same for each year, or at each elevation. While the empirical estimated long-wave irradiance at high-elevation sites resulted in melt rates lower than observations, at lower-elevations the same forcing caused mid-winter melt that was not observed. The higher sensitivity of simulated snowpacks at lower-elevation sites represents a difficult modeling environment that should be further used to test methods of generating forcing data as well as snow model formulation. For accumulated precipitation, the choice of which source was least biased, depended on the particular year. Future work remains to examine the impact of the sub-daily precipitation distribution between sources and the effect on the timing of snow accumulation and runoff.

GLOSSAARY OF ACRONYMS

Term	Definition
CDWR	The California Department of Water Resources
DHSVM	The Distributed Hydrology Soil and Vegetation Model
HMT	NOAA's Hydrometeorological Testbed
WRF	The Weather and Research Forecasting model
NARR	The North American Regional Reanalysis
NF American Basin	North Fork of the American River Basin
NSE	The Nash-Sutcliff efficency
PRISM	The Parameter Regression on Independent Slopes Model

REFERENCES

Anders, A. M., G. H. Roe, D. R. Durran, and J. R. Minder, 2007: Small-Scale Spatial Gradients in Climatological Precipitation on the Olympic Peninsula. *Journal of Hydrometeorology*, **8**, 1068–1081, doi:10.1175/JHM610.1. http://journals.ametsoc.org/doi/abs/10.1175/JHM610.1.

Andreadis, K. M., P. Storck, and D. P. Lettenmaier, 2009: Modeling snow accumulation and ablation processes in forested environments. *Water Resources Research*, **45**, 1–13, doi:10.1029/2008WR007042. http://www.agu.org/pubs/crossref/2009/2008WR007042.shtml (Accessed March 6, 2012).

Barros, A. P., and P. Lettenmaier, 1994: Dynamic modeling of orographically induced precipitation. *Reviews of Geophysics*, **32**, 265–284. http://www.agu.org/pubs/crossref/2009/2009JD011949.shtml.

Chin, H.-N. S., P. M. Caldwell, and D. C. Bader, 2010: Preliminary Study of California Wintertime Model Wet Bias. *Monthly Weather Review*, **138**, 3556–3571, doi:10.1175/2010MWR3409.1. http://journals.ametsoc.org/doi/abs/10.1175/2010MWR3409.1.

Daly, C., R. P. Neilson, and D. L. Phillips, 1994: A Statistical-Topographic Model for Mapping Climatological Precipitation over Mountainous Terrain. *Journal of Applied Meteorology*, **33**, 140–158, doi:10.1175/1520-0450(1994)033<0140:ASTMFM>2.0.CO;2. http://journals.ametsoc.org/doi/abs/10.1175/1520-0450%281994%29033%3C0140%3AASTMFM%3E2.0.CO%3B2.

Daly, C., W. Gibson, M. Doggett, J. Smith, and G. Taylor, 2004: A probabilistic-spatial approach to the quality control of climate observations. *Proceedings of the 14th AMS Conference on Applied*,.

Daly, C., M. Halbleib, J. I. Smith, W. P. Gibson, M. K. Doggett, G. H. Taylor, J. Curtis, and P. P. Pasteris, 2008: Physiographically sensitive mapping of climatological temperature and precipitation across the conterminous United States. *International Journal of Climatology*, **28**, 2031–2064, doi:10.1002/joc. http://onlinelibrary.wiley.com/doi/10.1002/joc.1688/abstract.

Das, T., M. D. Dettinger, D. R. Cayan, and H. G. Hidalgo, 2011: Potential increase in floods in California's Sierra Nevada under future climate projections. *Climatic Change*, **109**, 71–94, doi:10.1007/s10584-011-0298-z. http://www.springerlink.com/index/10.1007/s10584-011-0298-z (Accessed March 8, 2012).

Dettinger, M. D., 2005: Changes in Streamflow Timing in the Western United States in Recent Decades. *Sierra*, **3018**, 4.

Dettinger, M. D. and Coauthors, 2011: Design and quantification of an extreme winter storm scenario for emergency preparedness and planning exercises in California. *Natural Hazards*, **60**, 1085–1111, doi:10.1007/s11069-011-9894-5. http://www.springerlink.com/index/10.1007/s11069-011-9894-5 (Accessed March 8, 2012).

Dilley, A. C., and D. M. O'Brien, 1998: Estimating downward clear sky long-wave irradiance at the surface from screen temperature and precipitable water. *Quarterly Journal of the Royal*, 1391–1401. http://onlinelibrary.wiley.com/doi/10.1002/qj.49712454903/abstract (Accessed May 12, 2012).

Edwards, J. M., and A. Slingo, 1996: Studies with a flexible new radiation code. I: Choosing a configuration for a large-scale model. *Quarterly Journal of the Royal Meteorological Society*, **122**, 689–719, doi:10.1256/smsqj.53106. http://dx.doi.org/10.1002/qj.49712253107.

Flerchinger, G. N., W. Xaio, D. Marks, T. J. Sauer, and Q. Yu, 2009: Comparison of algorithms for incoming atmospheric long-wave radiation. *Water Resources Research*, **45**, 1–13, doi:10.1029/2008WR007394. http://www.agu.org/pubs/crossref/2009/2008WR007394.shtml (Accessed March 8, 2012).

Franklin, A. I., 1983: *Climate of the Priest River Experimental Forest , Northern Idaho*.

Hughes, M., and A. Hall, 2009: Local and synoptic mechanisms causing Southern California's Santa Ana winds. *Climate Dynamics*, **34**, 847–857, doi:10.1007/s00382-009-0650-4. http://www.springerlink.com/index/10.1007/s00382-009-0650-4.

Kimball, B. A., S. B. Idso, and J. K. Aase, 1982: A model of thermal radiation from partly cloudy and overcast skies. *Water Resources Research*, **18**, 931–936, doi:10.1029/WR018i004p00931. http://www.agu.org/pubs/crossref/1982/WR018i004p00931.shtml.

Kuraś, P. K., Y. Alila, M. Weiler, D. Spittlehouse, and R. Winkler, 2011: Internal catchment process simulation in a snow-dominated basin: performance evaluation with spatiotemporally variable runoff generation and groundwater dynamics. *Hydrological Processes*, **25**, 3187–3203, doi:10.1002/hyp.8037. http://doi.wiley.com/10.1002/hyp.8037 (Accessed March 8, 2012).

Laramie, R. L., and J. D. Schaake, 1972: *Simulation of the Continuous Snowmelt Process*. Mass. Inst. of Technol, Cambridge,.

Leung, L. R., M. S. Wigmosta, S. J. Ghan, D. J. Epstein, and L. W. Vail, 1996: Application of a subgrid orographic precipitation / surface hydrology scheme to a mountain watershed. **101**.

Lundquist, J., B. Huggett, H. Roop, and N. Low, 2009: Use of spatially distributed stream stage recorders to augment rain gages by identifying locations of thunderstorm precipitation and

distinguishing rain from snow. *Water Resources Research*, **45**, 1–7, doi:10.1029/2008WR006995. http://www.agu.org/pubs/crossref/2009/2008WR006995.shtml (Accessed March 8, 2012).

Lundquist, J. D., and B. Huggett, 2008: Evergreen trees as inexpensive radiation shields for temperature sensors. *Water Resources Research*, **44**, 1–5, doi:10.1029/2008WR006979. http://www.agu.org/pubs/crossref/2008/2008WR006979.shtml.

Lundquist, J. D., D. R. Cayan, and M. D. Dettinger, 2003: Meteorology and Hydrology in Yosemite National Park : A Sensor Network Application. *Sierra*, **2634**, 518–528. http://portal.acm.org/citation.cfm?id=1766027.

Marks, D., and J. Dozier, 1992: Climate and Energy Exchange At the Snow Surface in the Alpine Region of the Sierra-Nevada .2. Snow Cover Energy-Balance. *Water Resources Research*, **28**, 3043–3054.

Marks, D., J. Kimball, D. Tingey, and T. Link, 1998: The sensitivity of snowmelt processes to climate conditions and forest cover during rain-on-snow : a case study of the 1996 Pacific Northwest. **1587**.

Marty, C., R. Philipona, C. Fr, and A. Ohmura, 2002: Altitude dependence of surface radiation fuxes and cloud forcing in the alps : results from the alpine surface radiation budget network. **155**.

Meehl, G., T. Stocker, and W. Collins, 2007: Global climate projections. http://scholar.google.com/scholar?hl=en&btnG=Search&q=intitle:Global+Climate+Projections#0 (Accessed May 2, 2012).

Meek, D. W., and J. L. Hatfield, 1994: Data quality checking for single station meteorological databases I. *Agricultural and Forest Meteorology*, **1923**.

Mesinger, F., G. DiMego, and E. Kalnay, 2006: North American regional reanalysis. *of the American*,http://climateknowledge.org/reanalysis/Mesinger_NARR_regional_BAMS_2006.pdf (Accessed May 12, 2012).

Minder, J. R., D. R. Durran, and G. H. Roe, 2011: Mesoscale Controls on the Mountainside Snow Line. *Journal of the Atmospheric Sciences*, **68**, 2107–2127, doi:10.1175/JAS-D-10-05006.1. http://journals.ametsoc.org/doi/abs/10.1175/JAS-D-10-05006.1.

Mizukami, N., and M. B. Smith, 2012: Analysis of inconsistencies in multi-year gridded quantitative precipitation estimate over complex terrain and its impact on hydrologic modeling. *Journal of Hydrology*, **428-429**, 129–141, doi:10.1016/j.jhydrol.2012.01.030. http://linkinghub.elsevier.com/retrieve/pii/S002216941200073X.

Morrison, H., G. Thompson, and V. Tatarskii, 2009: Impact of Cloud Microphysics on the Development of Trailing Stratiform Precipitation in a Simulated Squall Line: Comparison of One- and Two-Moment Schemes. *Monthly Weather Review*, **137**, 991–1007, doi:10.1175/2008MWR2556.1. http://journals.ametsoc.org/doi/abs/10.1175/2008MWR2556.1.

Mote, P. W., A. F. Hamlet, M. P. Clark, and D. P. Lettenmaier, 2005: Declining Mountain Snowpack in Western North America, *Bulletin of the American Meteorological Society*, **86**, 39–49, doi:10.1175/BAMS-86-1-39. http://journals.ametsoc.org/doi/abs/10.1175/BAMS-86-1-39 (Accessed March 5, 2012).

Nijssen, B., D. P. Lettenmaier, X. Liang, S. W. Wetzel, and E. F. Wood, 1997: Streamflow simulation for continental-scale river basins. *Water Resources Research*, **33**, 711–724, doi:10.1029/96WR03517. http://www.agu.org/pubs/crossref/1997/96WR03517.shtml.

Pomeroy, J., D. Marks, T. Link, and C. Ellis, 2009: The impact of coniferous forest temperature on incoming longwave radiation to melting snow. *Hydrological*, doi:10.1002/hyp. http://onlinelibrary.wiley.com/doi/10.1002/hyp.7325/abstract (Accessed May 2, 2012).

Prata, A. J., 1996: A new long-wave formula for estimating downward clear-sky radiation at the surface. *Quarterly Journal of the Royal Meteorological Society*, **122**, 1127–1151, doi:10.1002/qj.49712253306. http://doi.wiley.com/10.1002/qj.49712253306.

Ralph, F. M. and Coauthors, 2005: Improving Short-Term (0–48 h) Cool-Season Quantitative Precipitation Forecasting: Recommendations from a USWRP Workshop. *Bulletin of the American Meteorological Society*, **86**, 1619–1632, doi:10.1175/BAMS-86-11-1619. http://journals.ametsoc.org/doi/abs/10.1175/BAMS-86-11-1619.

Reed, S., V. Koren, M. Smith, Z. Zhang, F. Moreda, D.-J. Seo, and and DMIP Participants, 2004: Overall distributed model intercomparison project results. *Journal of Hydrology*, **298**, 27–60, doi:10.1016/j.jhydrol.2004.03.031. http://linkinghub.elsevier.com/retrieve/pii/S0022169404002380 (Accessed March 10, 2012).

Ruiz-Arias, J. a., D. Pozo-Vázquez, V. Lara-Fanego, F. J. Santos-Alamillos, and J. Tovar-Pescador, 2011: A High-Resolution Topographic Correction Method for Clear-Sky Solar Irradiance Derived with a Numerical Weather Prediction Model. *Journal of Applied Meteorology and Climatology*, **50**, 2460–2472, doi:10.1175/2011JAMC2571.1. http://journals.ametsoc.org/doi/abs/10.1175/2011JAMC2571.1 (Accessed May 12, 2012).

Running, S. W., R. R. Nemani, and R. D. Hungerford, 1987: Extrapolation of synoptic meteorological data in mountainous terrain and its use for simulating forest evapotranspiration and photosynthesis. *Canadian Journal of Forest Research.* **17,** 472-483.

Sevruk, B., 1983: Correction of Measured Precipitation in the Alps Using the Water Equivalent of New Snow. *Weather*, **14**, 49–58. http://www.iwaponline.com/nh/014/0049/0140049.pdf.

Shamir, E., and K. P. Georgakakos, 2006: Distributed snow accumulation and ablation modeling in the American River basin. *Advances in Water Resources*, **29**, 558–570, doi:10.1016/j.advwatres.2005.06.010. http://linkinghub.elsevier.com/retrieve/pii/S0309170805001727 (Accessed March 8, 2012).

Sicart, J. E., J. W. Pomeroy, R. L. H. Essery, and D. Bewley, 2006: Incoming longwave radiation to melting snow : observations , sensitivity and estimation in northern environments. **3708**, 3697–3708, doi:10.1002/hyp.

Skamarock, W., and J. Klemp, 2008: A time-split nonhydrostatic atmospheric model for weather research and forecasting applications. *Journal of Computational Physics*, **227**, 3465–3485, doi:10.1016/j.jcp.2007.01.037. http://linkinghub.elsevier.com/retrieve/pii/S0021999107000459 (Accessed July 27, 2011).

Soil Survey Staff, Natural Resources Conservation Service, United States Department of Agriculture, 2006: U.S. General Soil Map (STATSGO2) for California. [Available online at http://soildatamart.nrcs.usda.gov.]

Surfleet, C. G., A. E. S. Iii, and M. W. Meadows, 2011: Road runoff and sediment sampling for determining road sediment yield at the watershed scale. *Methods*, **1980**, 1970–1980, doi:10.1139/X11-104.

Thornton, P. E., and S. W. Running, 1999: An improved algorithm for estimating incident daily solar radiation from measurements of temperature , humidity , and precipitation. *Agricultural and Forest Meteorology*, **93**.

Tobin, C., L. Nicotina, M. B. Parlange, A. Berne, and A. Rinaldo, 2011: Improved interpolation of meteorological forcings for hydrologic applications in a Swiss Alpine region. *Journal of Hydrology*, **401**, 77–89, doi:10.1016/j.jhydrol.2011.02.010. http://linkinghub.elsevier.com/retrieve/pii/S0022169411001156 (Accessed July 19, 2011).

United States Geological Survey Land Cover Institute, 2005: California Land Cover data, [Available online at http://landcover.usgs.gov/.]

Waichler, S. R., and M. S. Wigmosta, 2003: Development of Hourly Meteorological Values From Daily Data and Significance to Hydrological Modeling at H. J. Andrews Experimental Forest. *Journal of Hydrometeorology*, **4**, 251–263, doi:10.1175/1525-7541(2003)4<251:DOHMVF>2.0.CO;2.

Weingartner, R., and C. Pearson, 2001: A Comparison of the Hydrology of the Swiss Alps and the Southern Alps of New Zealand. **21**, 370–381.

Westrick, K., 2001: An evaluation of a high-resolution hydrometeorological modeling system for prediction of a cool-season flood event in a coastal mountainous watershed. *Journal of Hydrometeorology*, **161**, 161–180. http://journals.ametsoc.org/doi/pdf/10.1175/1525-7541(2001)002%3C0161%3AAEOAHR%3E2.0.CO%3B2 (Accessed May 2, 2012).

Westrick, K., and P. Storck, 2002: Description and evaluation of a hydrometeorological forecast system for mountainous watersheds. *Weather and forecasting*, 250–262. http://journals.ametsoc.org/doi/abs/10.1175/1520-0434(2002)017%3C0250%3ADAEOAH%3E2.0.CO%3B2 (Accessed May 2, 2012).

Whitaker, A., Y. Alila, J. Beckers, and D. Toews, 2003: Application of the distributed hydrology soil vegetation model to Redfish Creek, British Columbia: model evaluation using internal

catchment data. *Hydrological Processes*, **17**, 199–224, doi:10.1002/hyp.1119. http://doi.wiley.com/10.1002/hyp.1119.

Wigmosta, M. S., B. Nijssen, P. Storck, and D. Lettenmaier, 1994: The distributed hydrology soil vegetation model. *Water Resource Publications,* 1–29.

Zhao, Q., 2009: The snowmelt runoff forecasting model of coupling WRF and DHSVM. *Hydrology and Earth System Sciences*, **13,** 1897-1906.

Appendix A: Observational stations used in this study.

Variable	Network	Number of Stations	Period of record	Temporal resolution
Precipitation	CDWR	4	1999-2010	Daily
	HMT	6	2007-2010	2-minute
Air temperature	CDWR	8	1999-2010	Daily
	HMT	8	2007-2010	2-minute
	iButtons	47	2008-2010	30-minute
Relative humidity	HMT	13	2007-2010	2-minute
	iButtons	52	2008-2010	30-minute
Wind Speed	CDWR	1	1999-2010	Daily
Short-wave irradiance	HMT	2	2007-2010	2-minute
	DRI	1	2007-2010	10-minute
Net irradiance	HMT	3	2007-2010	2-minute
Streamflow	USGS #11427000 NF Dam	1	1999-2010	Daily
	Sub-basin Stage height	2	2007-2010	Hourly
Snow water equivalent (SWE)	CDWR	6	1999-2010	Daily
	SNOTEL	2	1999-2010	Daily

Appendix B: Filling of temperature sensor gaps

Because the self-recording temperature sensors (iButtons) were placed in trees, they occasionally become covered in snow, resulting in low diurnal temperature ranges that have a mean near zero degrees. Any day that exhibited this type of behavior was removed from the data set. However, because these days are unrepresentatively cold, their removal introduces a warm bias to long-term means. Therefore, we employed empirical orthogonal function (EOF) reconstruction as described by von Storch and Zwiers (1999) and Beckers and Rixen (2003), in order to estimate some periods of missing temperature data. Filling of missing data via EOF reconstruction was only applied to those stations that recorded data at least 90% of each October-June period between 2008 and 2010. The resulting quality controlled and filled temperature data was then aggregated into monthly means if 90% of each month's hourly values were present. This method expands the available temperature data set while guaranteeing that wet season (October-June) means do not suffer from warm biases.

Appendix C: Fractional long-wave irradiance calculation under a canopy

Under a canopy the long-wave irradiance reaching the surface is calculated within DHSVM by Equation 1. Where ↓LW is the long-wave irradiance emitted from the viewable atmospheric column, F_{Canopy} is the fractional coverage of the canopy, and LW_{Canopy} is the long-wave irradiance emitted from the canopy. More complicated methods exists but are not tested here (Sicart et al. 2006).

Equation 1 $$LW_{SRF} = \downarrow LW * (1 - F_{Canopy}) + LW_{Canopy} * F_{Canopy}$$